Atmos. Chem. Phys. Discuss., 15, 15711–15753, 2015
www.atmos-chem-phys-discuss.net/15/15711/2015/
doi:10.5194/acpd-15-15711-2015

Atmospheric Chemistry and Physics Discussions
Open Access

Post bubble-closeoff fractionation of gases in polar firn and ice cores: effects of accumulation rate on permeation through overloading pressure

T. Kobashi[1,2,3], T. Ikeda-Fukazawa[4], M. Suwa[5], J. Schwander[1,2], T. Kameda[6], J. Lundin[7], A. Hori[6], M. Döring[1,2], and M. Leuenberger[1,2]

[1]Climate and Environmental Physics, University of Bern, Bern, Switzerland
[2]Oeschger Center for Climate Change Research, University of Bern, Bern, Switzerland
[3]National Institute of Polar Research, Tokyo, Japan
[4]Deparment of Applied Chemistry, Meiji University, Kanagawa, Japan
[5]The World Bank, Washington DC, USA
[6]Department of Civil and Environmental Engineering, Kitami Institute of Technology, Kitami, Japan
[7]Departement of Earth and Space Sciences, University of Washington, Seattle, USA

Received: 27 April 2015 – Accepted: 19 May 2015 – Published: 11 June 2015

Correspondence to: T. Kobashi (kobashi@climate.unibe.ch)

Published by Copernicus Publications on behalf of the European Geosciences Union.

Abstract

Gases in ice cores are invaluable archives of past environmental changes (e.g., the past atmosphere). However, gas fractionation processes after bubble closure in the firn are poorly understood, although increasing evidence indicates preferential leakages of smaller molecules (e.g., neon, oxygen, and argon) from the closed bubbles through ice crystals. These fractionation processes are believed to be responsible for the observed millennial $\delta O_2/N_2$ variations in ice cores, linking ice core chronologies with orbital parameters. Herein, we found that $\delta Ar/N_2$ at decadal resolution on the gas age scale in the GISP2 ice core has a significant negative correlation with accumulation rate over the past 6000 years. Furthermore, the precise temperature and accumulation rate records over the past 4000 years are found to have nearly equal effects on $\delta Ar/N_2$ with sensitivities of 0.72 ± 0.1 ‰ °C^{-1} and -0.58 ± 0.09 ‰ (0.01 m ice yr^{-1})$^{-1}$, respectively. To understand the fractionation processes, we applied a permeation model to "microbubbles (< 1 % of air content in the Vostok ice core)" and "normal bubbles" in the firn. The model indicates that $\delta Ar/N_2$ in the microbubbles is negatively correlated with the accumulation rate as found in the observation, due to changes in overloading pressure. Colder (warmer) temperatures in the firn induce more (less) depletions in $\delta Ar/N_2$. The microbubbles are so depleted in $\delta Ar/N_2$ at the bubble closeoff depth that they dominate the total $\delta Ar/N_2$ changes in spite of their smaller volumes. The model also indicates that $\delta Ar/N_2$ of GISP2 and NGRIP should have experienced several permil of depletion during the storage 14 years after coring. Further understanding of the $\delta Ar/N_2$ and $\delta O_2/N_2$ fractionation processes in the firn may lead to a new proxy for the past temperature and accumulation rate.

1 Introduction

Atmospheric gases trapped in the firn layer (unconsolidated snow layer; ~ 70 m at the Greenland Summit) provide precious and continuous records of the past atmosphere and environments (Petit et al., 1999; Spahni et al., 2005; Ahn and Brook, 2008; Kobashi et al., 2008a). However, to reconstruct the original records, it is important to understand the processes of air trapping in the firn, and how the air is retained in the ice until it is analysed in laboratories. Two processes are well-known that change air composition before the air is trapped within bubbles in the firn. First, gravitational fractionation separates gases according to their mass differences and diffusive column height of the firn layer (Craig et al., 1988; Schwander, 1989). Second, a temperature gradient (ΔT) between the top and bottom of the firn layer induces thermal fractionation generally pulling heavier gases toward the colder end (Severinghaus et al., 1998). In this study, we investigate the third process that occurs after the bubbles are closed (post bubble closeoff fractionation) and that preferentially affects gases with smaller molecular sizes (< 3.6 Å; for example, helium, neon, oxygen, and argon), but also gases with larger molecular sizes in smaller magnitudes (Ikeda-Fukazawa et al., 2005; Huber et al., 2006; Ikeda-Fukazawa and Kawamura, 2006; Severinghaus and Battle, 2006; Ahn et al., 2008). This fractionation continues deep in ice sheets smoothing signals (Ahn et al., 2008; Bereiter et al., 2014), and the process further continues during/after coring (Ikeda-Fukazawa et al., 2005; Kobashi et al., 2008b; Suwa and Bender, 2008b; Bereiter et al., 2009; Vinther et al., 2009).

Clear evidence of the diffusive gas loss from ice cores has been observed in the oxygen content in ice cores as a rapid depletion of oxygen relative to nitrogen (Bender et al., 1995; Ikeda-Fukazawa et al., 2005; Suwa and Bender, 2008b). Depletion of air content by ~ 10 % was also observed for the Camp Century ice core after storage for 35 years, although possible analytical differences between early and late measurements cannot be rejected (Vinther et al., 2009). The process is highly temperature dependent, and it is induced by the pressure gradients between the bubbles and the atmosphere (Ikeda-Fukazawa et al., 2005). In ice sheets, the concentration gradients at different depths drive the gas diffusion, which smooth climate signals (Bereiter et al., 2014). Firn air studies showed that smaller molecules such as helium, neon, oxygen, and argon preferentially leak out from the closed bubbles, leading to enrichments of

ACPD
15, 15711–15753, 2015

these gases in open pores near the bubble-closeoff depth, which leads to depletions of lighter gases in the closed bubbles (Huber et al., 2006; Severinghaus and Battle, 2006; Battle et al., 2011). However, the mechanisms creating $\delta Ar/N_2$ or $\delta O_2/N_2$ variations in the time domain (i.e., ice cores) are still poorly understood.

$\delta O_2/N_2$ variations in the orbital scale are found to closely follow local insolation changes (Bender, 2002; Kawamura et al., 2007; Suwa and Bender, 2008a; Landais et al., 2012). As a possible mechanism, it has been hypothesized that changes in local insolation affect physical properties of the snow at the surface that persist into the bubble closeoff depth, controlling the $\delta O_2/N_2$ fractionation (insolation hypothesis) (Bender, 2002; Fujita et al., 2009). In addition, air content in ice cores are also found to covary with $\delta O_2/N_2$ in the orbital time scale, indicating common causes (Raynaud et al., 2007; Lipenkov et al., 2011). According to this hypothesis, the orbital signals in $\delta O_2/N_2$ in ice cores are locked in the ice chronology rather than in the gas chronology, which differ by up to a few thousand years. Therefore, the precise understanding of the gas loss process in the firn is essential to determine how climate signals in the bubbles are placed between the ice-ages and gas-ages on the orbital time scale.

In this paper, using $\delta Ar/N_2$ from GISP2 for the entire Holocene and from NGRIP for the past 2100 years, we investigated their multi-decadal to centennial variability, as well as the gas loss processes during the storage. $\delta Ar/N_2$ variations are generally highly correlated with $\delta O_2/N_2$ in ice cores, suggesting that similar processes for $\delta O_2/N_2$ that drive the $\delta Ar/N_2$ variations (Bender et al., 1995). As $\delta Ar/N_2$ is nearly constant in the atmosphere over the concerned period (Kobashi et al., 2010), it is better suited to assess the permeation processes in the firn and ice cores than $\delta O_2/N_2$ that varied in the atmosphere by ~ 1.5 ‰ during the glacial–interglacial cycles (Bender et al., 1995). In the following sections, we first describe the data, and investigate the relationships between $\delta Ar/N_2$ and changes in accumulation rates and surface temperatures. Then, the fractionation processes are examined by applying permeation models to the ice cores and the microbubbles and normal bubbles in the firn. Finally, we discuss our findings, draw conclusions and implications.

2 Data description

$\delta Ar/N_2$ was measured from the GISP2 ice core over the entire Holocene in an attempt to reconstruct the past surface temperatures from $\delta^{15}N$ and $\delta^{40}Ar$ (Kobashi et al., 2008b). The sample resolution varies from 10 to 20 years with high resolution analyses covering the past 1000 years (Kobashi et al., 2010) and around the 8.2ka event (8100 ± 500 years Before Present (BP, "Present" is defined as 1950)) (Kobashi et al., 2007). The sizes (50–100 g) of ice samples for this study (Kobashi et al., 2008b, 2015) were bigger than that (15–20 g) commonly used for $\delta^{15}N$ and $\delta O_2/N_2$ measurements (Bender et al., 1995; Suwa and Bender, 2008b). The larger sample size is important to obtain high precision for analytical purposes (Kobashi et al., 2008b) and to minimize the effect of the inhomogeneity in an ice sample (Headly, 2008). For the time scale, we used the GICC05 (Vinther et al., 2006; Seierstad et al., 2014). To calculate gas ages, a firn densification-heat diffusion model (Goujon et al., 2003) was applied, and the uncertainties were estimated as ~ 10 % of the gas-ice age difference (Goujon et al., 2003). We used reconstructed temperature records from argon and nitrogen isotopes in the trapped air within the GISP2 ice core for the past 4000 years and NGRIP for the past 2100 years (Kobashi et al., 2011), and layer-counted accumulation rate data for the entire Holocene (Alley et al., 1997; Cuffey and Clow, 1997; Gkinis et al., 2014) to investigate the $\delta Ar/N_2$ fractionation, and the annual resolution accumulation rate data were smoothed with 21 years running means (RMs) to mimic gas diffusion and the bubble closeoff process in the firn.

Similarly, new NGRIP $\delta Ar/N_2$ data for the past 2100 years from the NGRIP ice core were also investigated in this study, providing a good comparison with the GISP2 data. The current NGRIP site has a similar mean annual air temperature of around −30 °C with GISP2. However, the accumulation rate at NGRIP is 20 % lower than that of GISP2 over the past 2100 years, and importantly its variations (standard deviation after 21 years RMs) are lower by 40 % than that of GISP2 (see later discussion).

The conventional delta notation is used to express $\delta Ar/N_2$ as follows:

$$\delta Ar/N_2 = \left[(Ar/N_2)_{sample}/(Ar/N_2)_{standard} - 1\right] 10^3 \text{ (‰)} \quad (1)$$

where the subscript "sample" indicates ice core values, and "standard" is the present atmospheric composition. For GISP2, mass 40 of argon and 29 of nitrogen, and for NGRIP, mass 40 of argon and 28 of nitrogen were used to calculate $\delta Ar/N_2$. All $\delta Ar/N_2$ data presented in this study were corrected for gravitational and thermal fractionations in the firn using a conventional method (Severinghaus and Battle, 2006; Severinghaus et al., 2009) with $\delta^{15}N$ for GISP2 as follows:

$$\delta Ar/N_{2gravcorr} = \delta Ar/N_2 - 11\delta^{15}N \quad (2)$$

The coefficient 11 is derived as the mass difference of $\delta Ar/N_2$ (^{40}Ar and $^{29}N_2$) is 11 times larger than that of the nitrogen isotopes ($^{29}N_2$ and $^{28}N_2$) for GISP2. This coefficient is replaced with 12 for the calculation of $\delta Ar/N_{2gravcorr}$ for NGRIP because the mass difference between ^{40}Ar and $^{28}N_2$ is 12. As the temperature sensitivity of $\delta^{15}N$ and $\delta Ar/N_2$ is slightly different, the correction is not perfect. However, the variability induced by the gas loss is much bigger than the uncertainties introduced by the differences of the thermal sensitivities. Therefore, these corrections work well. After these corrections, the $\delta Ar/N_2$ variations in the ice cores can be attributed only to the process of the gas loss. It is also noted that $\delta Ar/N_{2gravcorr}$ of the GISP2 data using the mass 28 or 29 leads to negligible differences (an average difference is 0.4×10^{-3} ‰ and the standard deviation is 0.94×10^{-3} ‰), which is much smaller than the measurement uncertainty (> 0.5 ‰) of $\delta Ar/N_2$.

A spline fit (Enting, 1987) was applied to the $\delta Ar/N_2$ data with a 21 years cut off period, and used for the following analyses to investigate signals longer than the multidecadal period. The significances of correlations were calculated considering the autocorrelation of time series (Ito and Minobe, 2010; Kobashi et al., 2013). We consider > 95 % confidence as significant, unless otherwise noted.

3 GISP2 $\delta Ar/N_2$ variation over the Holocene

The $\delta Ar/N_2$ record over the Holocene in the GISP2 ice core exhibits relatively constant values around −3 ‰, except for a prominent rise of up to 10 ‰ around 7000 BP (Fig. 1). The rise is located within the depths of the brittle zone (650–1400 m) where air in the bubbles changes to clathrate inducing anomalously high pressure (Gow et al., 1997). The dissociation pressure of nitrogen in the clathrate phase is higher than that of argon (or oxygen) so that nitrogen is enriched in the gas phase in relation to the clathrate (more stable state), resulting in a preferential leakage of nitrogen, leading to argon (or oxygen) enrichments in these depths (Ikeda et al., 1999; Ikeda-Fukazawa et al., 2001; Kobashi et al., 2008b). As the dissociation of gases from the clathrate depends on various factors, $\delta Ar/N_2$ in these depths are highly variable (Fig. 1). It is noted that $\delta^{15}N$ and $\delta^{40}Ar$ do not exhibit influences from the anomalous $\delta Ar/N_2$ fractionation, indicating that the processes are mass independent in first order (Huber et al., 2006; Severinghaus and Battle, 2006) (Fig. 1).

Changes in the surface temperatures and accumulation rates are the dominant controlling factors for the state of firn layers (e.g., density profile, bubble closeoff depth, and firn thickness) (Herron and Langway, 1980; Schwander et al., 1997; Goujon et al., 2003). Therefore, we investigated if changes in surface temperature or accumulation rate have any control on the $\delta Ar/N_2$ variations. Then, a significant negative correlation ($r = -0.29$, $p = 0.03$) between $\delta Ar/N_2$ on the gas age scale and the accumulation rate was found for the past 6000 years when the abnormal $\delta Ar/N_2$ fractionation is not observed (Figs. 1 and 2). This negative correlation is opposite of what an earlier study (Severinghaus and Battle, 2006) suggested for the permeation fractionation in the firn (positive correlation). In addition, the significant correlation was found for $\delta Ar/N_2$ on the "gas ages" scale rather than the "ice ages" that the insolation hypothesis predicts; an indication that new processes need to be considered for the gas loss processes in the firn.

ACPD
15, 15711–15753, 2015

GISP2 data for the past 4000 years provide a unique opportunity to investigate $\delta Ar/N_2$ variations as precise temperature (Kobashi et al., 2011) and accumulation rate records (Alley et al., 1997; Cuffey and Clow, 1997) are available. Using these data, we applied a linear regression and lag analysis on $\delta Ar/N_2$. It is found that the surface temperature is positively correlated with $\delta Ar/N_2$ on the gas ages ($r = 0.47$, $p = 0.04$; $r = 0.28$, $p = 0.001$ after linear detrending) with a 68 years lag (Fig. 3a), indicating that cooler (warmer) temperatures induced more (less) depletions in $\delta Ar/N_2$ with a multidecadal lag. On the other hand, the accumulation rate is negatively correlated with $\delta Ar/N_2$ on the gas ages ($r = -0.47$, $p = 0.12$; $r = 0.26$, $p = 0.01$ after linear detrending) with a 38 years lag (Fig. 3b), indicating that high (low) accumulation rates induced more (less) depletions in $\delta Ar/N_2$ over the past 4000 years. It is noted that the surface temperature and accumulation rate have a weak negative but insignificant correlation ($r = -0.32$, $p = 0.13$; after linear detrending $r = -0.11$, $p = 0.2$) over the past 4000 years.

To estimate the relative contribution of the accumulation rate and the surface temperature changes on $\delta Ar/N_2$, we applied a multiple linear regression, which finds the best linear combination of variables (i.e., temperature and accumulation rate) for a response variable (i.e., $\delta Ar/N_2$). Before the regression is applied, the temperature and accumulation records were shifted toward younger ages to account for the lags (38 and 68 years for accumulation rate and temperature, respectively). As ordinary least squares including the multiple linear regression underestimate the variance of target time series when the data is noisy (Von Storch et al., 2004), we used "variance matching" by linearly scaling regression coefficients according to the ratio between the variance of the target and model time series. Figure 3c shows the original and modeled results of $\delta Ar/N_2$ over the past 4000 years. As expected, the model of the multiple linear regression captures the $\delta Ar/N_2$ variations better than the individual variables do (Fig. 3a–c) with a correlation coefficient of $r = 0.58$, $p = 0.09$ ($r = 0.36$, $p < 0.001$ after linear detrending). For the centennial variations, the model captures nearly half of the total variance of the observed $\delta Ar/N_2$ variations with a 95 % confidence ($r = 0.71$, $p = 0.05$ after linear detrending with 200 years RMs). The high and significant correlation between the model and observed $\delta Ar/N_2$ indicates that changes in the surface temperature and accumulation rate played important roles in controlling the $\delta Ar/N_2$ variations. The sensitivities of $\delta Ar/N_2$ on the changes in the temperatures and the accumulation rates were estimated to be 0.72 ± 0.1 ‰ °C^{-1} and -0.58 ± 0.09 ‰ $(0.01\,m\,yr^{-1})^{-1}$, respectively.

Next, we attempted to use oxygen isotopes of ice ($\delta^{18}O_{ice}$) as a temperature proxy for the same regression analyses of $\delta Ar/N_2$ since we do not have the precise temperature information before the past 4000 years BP. Although a $\delta^{18}O_{ice}$ record from an ice core contains large noises that could be transferred to an estimated temperature record, stacking several $\delta^{18}O_{ice}$ records reduces the noises and provides a better temperature record (White et al., 1997; Kobashi et al., 2011). Thus, we stacked three oxygen isotope records (GISP2, GRIP, and NGRIP) over the Holocene in the 20 years RMs (Stuiver et al., 1995; Vinther et al., 2006). The stacked record was calibrated to temperatures using the relation obtained from borehole temperature profiles (Cuffey and Clow, 1997). Using the regression coefficients obtained earlier (Fig. 3c), a $\delta Ar/N_2$ model was calculated from the oxygen-isotope-based temperature and the accumulation rate (Fig. 3d). We found that the correlation between the model and the observed $\delta Ar/N_2$ performs not as well as the one with the temperature and accumulation rate for the past 4000 years (Fig. 3c), but does slightly better than the correlations with the temperature or accumulation rate, individually (Fig. 3a, b).

The $\delta Ar/N_2$ regression model with the $\delta^{18}O_{ice}$ and accumulation rate can span the entire Holocene, including the periods when the observed $\delta Ar/N_2$ are highly variable owing to the post coring fractionation as discussed earlier. The model and observed $\delta Ar/N_2$ except the time window around ~ 7000 BP exhibit rather constant values of 3–4 ‰ throughout the Holocene (Fig. 4). Interestingly, the model indicates that the constant $\delta Ar/N_2$ during the early Holocene is the result of a cancellation between the effects of the accumulation rate and the temperature, both of which were rapidly rising in the early Holocene (Fig. 4). The $\delta Ar/N_2$ variations remained higher or noisier from

ACPD
15, 15711–15753, 2015

the early Holocene to ~ 6000 BP than that for the later period, which probably made it difficult to decipher the original multidecadal to centennial signals in $\delta Ar/N_2$ (Fig. 4).

4 NGRIP $\delta Ar/N_2$ variation over the past 2100 years

$\delta Ar/N_2$ of the NGRIP ice cores provides a good comparative dataset with the GISP2 data (Fig. 5). Average $\delta Ar/N_2$ for the past 2100 years are −6.12 and −3.90 ‰ for NGRIP and GISP2, respectively (Fig. 5). The $\delta Ar/N_2$ variability in NGRIP (1σ = 0.75 ‰) over the past 2100 years is about 40 % smaller than that of GISP2 (1σ = 1.21 ‰), likely owing to the smaller variations of the accumulation rate at NGRIP than that of GISP2 (Fig. 5). The pooled standard deviations of replicated samples are 0.94 ‰ for NGRIP over the past 2100 years, and 0.66 ‰ for GISP2 over the past 1000 years (replicates are available only for the past 1000 years in GISP2) (Kobashi et al., 2008b). The noisier data for NGRIP than that for GISP2 should not be analytical as the mass spectrometer used for the NGRIP had better precision on $\delta Ar/N_2$ than that for the GISP2 (Kobashi et al., 2008b, 2015). $\delta Ar/N_2$ for GISP2 and NGRIP are only marginally correlated with a correlation coefficient of $r = 0.22$ ($p = 0.07$) for the overlapping period, but the centennial variations (with 100 years RMs) exhibit a more significant correlation ($r = 0.44$, $p = 0.04$ after linear detrending). The surface temperatures at NGRIP were only weakly correlated with $\delta Ar/N_2$ in the deeper part of NGRIP ($r = 0.20$, $p = 0.06$ after linear detrending) but not in the shallower part. No significant correlations were found between $\delta Ar/N_2$ and the accumulation rate for NGIRP, probably due to the lower variation of the accumulation rate at NGRIP than that of GISP2.

$\delta Ar/N_2$ record from the depth of 64.6–80 m exhibits some interesting features (Fig. 6). The depth from ~ 60 to 78 m corresponds to the lock-in zone in NGRIP, where vertical mixing of gas is limited so that $\delta^{15}N$ stays nearly constant in these depths (Huber et al., 2006; Kawamura et al., 2006). Therefore, the shallowest data at 64.6 m are located in the lock-in zone (Fig. 6). Generally, gas data from the lock-in zone are not used owing to possible contamination. However, a recent study (Mitchell et al., 2015) demonstrated that $\delta^{15}N$ can be used to estimate the amount of contaminations, and the original methane concentration in the firn was reconstructed with a range of uncertainties from ice samples in the lock-in zone. Therefore, we interpreted the observed rapid decreases of $\delta^{15}N$ and $\delta^{40}Ar$ in the lock-in-zone as the result of mixing with ambient air (Fig. 6). Considering the isotope mass balance, we calculated the original $\delta Ar/N_2$ values, which exhibited highly depleted values as low as −50 ‰ (Fig. 6). The depleted $\delta Ar/N_2$ in the lock-in-zone provides a clue for the processes of gas loss in the firn (see later discussion).

5 Process study I: $\delta Ar/N_2$ permeation model and application to the fractionation during the storage

To quantitatively evaluate changes in gas composition after the coring, we applied a molecular diffusion model (permeation model) on the ice cores (Ikeda-Fukazawa et al., 2005). This model has been applied to observed oxygen depletions by ∼ 10 ‰ in the Dome Fuji and GISP2 ice cores (Ikeda-Fukazawa et al., 2005; Suwa and Bender, 2008b). The model has also been implemented with modifications for gas permeation processes in the firn (Severinghaus and Battle, 2006) and in ice cores (Bereiter et al., 2009). The gas permeation from ice cores is driven by the pressure gradients in the bubbles and the atmosphere. The concentration (U_m; $\mathrm{mol\,mol_{ice}^{-1}}$) of m molecule (i.e., nitrogen, oxygen, and argon) in bubbles in one mole of ice after a time t can be described as follows (Ikeda-Fukazawa et al., 2005):

$$U_m = U_m^0 - k_m X_m \left(P^i Z_m^i - P^a Z_m^s\right) S/V t \quad (3)$$

where U_m^0 ($\mathrm{mol\,mol_{ice}^{-1}}$) is the original concentration of m molecule. k_m ($\mathrm{m\,s^{-1}}$) is the mass transfer coefficient and equals to $D_m/\Delta l$, where D_m ($\mathrm{m^2\,s^{-1}}$) is the diffusion coefficient of the m molecule, and Δl (m) is the thickness of the surface layer of ice (Ikeda-Fukazawa et al., 2005). X_m ($\mathrm{mol\,mol_{ice}^{-1}\,MPa^{-1}}$) is the solubility of m molecule in

ACPD
15, 15711–15753, 2015

ice. P^i and P^a are the pressures in the bubbles and in the atmosphere, respectively. Z_m^i and Z_m^s are molar fractions of m molecule in the bubbles and in the atmosphere, respectively. S (m^2) and V (m^3) represent the surface area and the volume of an ice sample such that S/V can be understood as specific surface area (m^{-1}), an important variable for the gas exchange between the atmosphere and the ice (Matzl and Schneebeli, 2006).

In this study, we applied the model to estimate argon loss from the ice cores during the storage. Coincidentally, both GISP2 and NGRIP ice cores were analysed for $\delta Ar/N_2$ ~ 14 years after the coring, however, with different temperature histories. The GISP2 (82.4–540 m) was cored in summer 1991. After the shipment, the cores were stored at −29 °C in a commercial freezer until they were moved to a freezer (−36 °C) at the National Ice Core Laboratory (NICL) in February 1993 (G. Hargreaves, personal communication, 2015). Then, the ice samples were cut and moved to the Scripps Institution of Oceanography where $\delta Ar/N_2$ was measured in 2005 (Kobashi et al., 2008b). One the other hand, the NGRIP2 ice cores (64.6–445.2 m) were cored in summer 1999 (Dahl-Jensen et al., 2002). Shallower parts (64.6–254.4 m) were stored in a freezer at the University of Copenhagen around −24 °C (J. P. Steffensen, personal communication, 2015), and deeper parts (255.5–445.2 m) were in a freezer of a commercial facility rented by the Alfred Wegener Institute (AWI) at −30 °C (S. Kipfstuhl, personal communication, 2015). In fall 2011, we cut the ice samples, and shipped them to a freezer at the National Institute of Polar Research at −30 °C until 2013 when we analysed the ice cores (Kobashi et al., 2015).

We assumed an initial air content of 6.53×10^{-5} mole in one mole of ice (a typical air content in ice cores), and bubble pressures P^i to 1 MPa that is a normal bubble pressure at 200 m depth for Vostok (Lipenkov, 2000). U_m^0 for each gas is calculated from the total gas content multiplied by the atmospheric molar ratio of each gas. In this case, Z_m^i and Z_m^s are set to the atmospheric partial pressures for each molecule. Another factor that affects the gas loss is the specific surface area. The GISP2 cores had a larger diameter (0.132 m) and longer length (1 m) during the storage than that (diameter 0.098 m and length 0.55 m) of NGRIP. Therefore, the specific surface areas (S/V) were calculated to be 32.3 and 44.5 m^{-1} for GISP2 and NGRIP, respectively. It is noted that these specific surface areas are approximations as ice cores during the storage have often different shapes, and we shaved the ice surface by ∼ 5 mm before the analyses (Kobashi et al., 2008b, 2015). The temperature histories and the specific surface areas indicate that the NGRIP ice cores were more susceptible to the gas loss during storage.

To calculate argon diffusion from the ice cores, it is necessary to estimate the solubility and diffusivity of argon in ice at different temperatures. However, diffusion coefficients of argon are only available at 270 K (D_{Ar}; $4.0\times10^{-11}\,m^2\,s^{-1}$) with those of nitrogen (D_{N_2}; $2.1\times10^{-11}\,m^2\,s^{-1}$) and oxygen ($D_{O_2}$; $4.7\times10^{-11}\,m^2\,s^{-1}$) from molecular dynamics simulations (Ikeda-Fukazawa et al., 2004). Therefore, we estimated k_{Ar} and X_{Ar} assuming that the geometrical relationship between D_{N_2}, D_{Ar}, and D_{O_2} at 270 K holds for k_m and X_m at different temperatures. This leads to the following equations (Fig. 7).

$$k_{Ar} = k_{O_2} - (4.7-4.0)/(4.7-2.1)(k_{O_2} - k_{N_2}) \quad (4)$$

$$X_{Ar} = X_{O_2} - (4.7-4.0)/(4.7-2.1)(X_{O_2} - X_{N_2}) \quad (5)$$

X_m and k_m for nitrogen and oxygen in different temperatures can be calculated through Eqs. (4) and (8) in Ikeda-Fukazawa et al. (2005). This leads to estimates of $k_{Ar}X_{Ar}$ (= permeability/Δl) (Fig. 7). Using these values, the gas loss of each gas was calculated from Eq. (3) with different temperature histories, and expressed by the standard delta notation relative to the atmospheric values. Then, it is found that $\delta Ar/N_2$ should be depleted in relation to the original values by −2.7, −6.6, and −4.4 ‰ for GISP2, NGRIP shallow, and NGRIP deep, respectively. The observed average $\delta Ar/N_2$ of GISP2, NGRIP shallow, and NGRIP deep over the past 2100 years are −3.9, −6.3, and −6.0 ‰ (Fig. 5), indicating that $\delta Ar/N_2$ before the storage had the values of −1.2, 0.3, and −1.6 ‰, respectively. It is noted that a large gap in the calculated original $\delta Ar/N_2$ between the shallow and deep NGRIP ice cores and in particular the positive

Discussion Paper | Discussion Paper | Discussion Paper | Discussion Paper |
ACPD
15, 15711–15753, 2015
Post bubble-closeoff fractionation of gases in polar firn and ice cores
T. Kobashi et al.

value for the NGRIP shallow, may indicate that the estimated permeability is possibly several folds larger than that in the real world.

The larger depletion in $\delta Ar/N_2$ from the NGRIP ice core likely introduced noises into the original $\delta Ar/N_2$ signals, causing poorer reproducibility in the NGRIP data than that of the GISP2 data, which likely made it difficult to attribute the NGRIP $\delta Ar/N_2$ variation to changes in surface temperature and/or accumulation rate. Ice cores during the storage often have different shapes from earlier samplings, and have different micro-environments in boxes or freezers. All of these factors induce differential permeations for different ice pieces, and so introduce larger noises if the gas loss is more intense.

6 Process study II: post bubble-closeoff fractionation for micro- and normal bubbles

Air bubbles in the polar firn or ice can be categorized into two types (Lipenkov, 2000). The first one are normal bubbles and the other are so called microbubbles ($< 50\,\mu m$). They can be distinguished as a bimodal distribution in ice cores (Lipenkov, 2000; Ueltzhöffer et al., 2010; Bendel et al., 2013). The normal bubbles form at the bubble closeoff depth, and most of the air in ice cores is captured as the normal bubbles, and the air-trapping processes are relatively well known (Schwander et al., 1997; Goujon et al., 2003; Mitchell et al., 2015). On the other hand, the microbubbles are believed to form near the surface (Lipenkov, 2000). Therefore, they are highly pressurized and have rounded shape by the time when the bubbles reach the bubble closeoff depth (Lipenkov, 2000; Ueltzhöffer et al., 2010). Owing to the different histories of the bubbles in the firn (i.e., air pressures and duration in the firn after the closure), $\delta Ar/N_2$ or $\delta O_2/N_2$ in the microbubbles and normal bubbles should be different if the permeation theory is correct. Therefore, we attempted to quantify the processes of the gas loss from closed bubbles using a permeation model (Ikeda-Fukazawa et al., 2005) combined with the inputs from firn-densification heat-diffusion models (Schwander et al., 1997; Goujon et al., 2003).

6.1 Microbubbles

We first looked into the microbubble processes. Microbubbles are believed to form in the shallow firn by sublimation-condensation processes (Lipenkov, 2000). These bubbles have smaller sizes, smoothed spherical surfaces, and can generally be found in the interior of the ice crystals (Lipenkov, 2000). The air volume contribution of the microbubbles to the air content is estimated to be 0.3 % in the Vostok ice core (Lipenkov, 2000). Because microbubbles are formed in the shallow firn, air pressure in the microbubbles can reach levels as high as ice load pressure or slightly below at the bubble closeoff depth (Lipenkov, 2000). To model the gas permeation process from the microbubbles, we assumed steady state with given surface temperatures and accumulation rates, and calculated the ages, firn densities, porosities, and overloading pressures at given depths, using a firn densification-heat diffusion model (Schwander et al., 1997). Then, they are interpolated for annual layers in the firn for the following calculation.

Changes in the concentrations of m molecule were calculated according to the following Eq. (6) similar to Eq. (3).

$$U_m(l+1) = U_m(l) - k_m X_m \left(P^i(l) Z^i_m(l) - P^a Z^s_m\right) \left(\frac{S}{V}(l)\right) P_{open}(l) t C(l) \tag{6}$$

$$Z^i_m(l) = \frac{U_m(l)}{U_{Ar}(l) + U_{O_2}(l) + U_{N_2}(l)}$$

where l is an annual layer from the surface to deeper firn, and P_{open} is open pore ratio relative to the porosity (Fig. 8a). In a steady state, l can be considered as a time variable. At $l = 0$, the concerned microbubbles in an annual layer are at surface, although they are not active in terms of permeation at these depths (Fig. 8). With increasing l in a one year step, the microbubbles move deeper in the firn with l annual layers overlying. C is a coefficient defining the gas concentration in a concerned annual layer l relative to the total air in ice. It is assumed that the pressure $P^i(l)$ in the microbubbles start increasing with overloading pressure from the depth of the overloading pressure of 0.375 MPa (Fig. 8c), and that pressure changes were considered to be negligible above the depth. Initial P^i (0) was set at 0.065 MPa similar to the Greenland Summit (Schwander et al., 1993). We estimated the specific surface area (S/V) from the linear relationship between the specific surface areas (m^{-1}) and densities ρ from the Greenland Summit (Lomonaco et al., 2011) with an equation: S/V (m^{-1}) = $-16\,799\rho$ ($g\,cm^{-3}$) + 14 957. The initial gas content in the microbubbles was set at 1–3 % of the air content (6.53226×10^{-5} mole × 0.01) per 1 mole of ice, and it is composed of nitrogen (78.084 %), oxygen (20.9476 %), and argon (0.934 %). The specific surface area S/V was multiplied by P_{open} (Fig. 8a) as the gas loss occurs toward open pores.

Figure 8 shows model results with a temperature of −30 °C, an accumulation rate of 0.25 m ice yr^{-1}, and 1 % microbubble contribution. It shows that the gas permeation from the microbubbles starts soon after the pressure was applied to the microbubbles (Fig. 8c, d). As oxygen has a larger permeability than that of argon, $\delta O_2/N_2$ depletion is larger than $\delta Ar/N_2$ (Fig. 8b). At the temperature of −30 °C and accumulation rate of 0.25 m ice yr^{-1}, the depletion reaches up to ∼ 70 ‰ for $\delta Ar/N_2$, and ∼ 100 ‰ for $\delta O_2/N_2$ in the model, which leads to 5 % gas loss from the original air content of the microbubbles (Fig. 8c).

6.2 Normal bubbles

Most of the air in ice cores (∼ 99 %) is trapped as normal bubbles near the lock-in depth (Fig. 9a). As a result, bulk air pressure in the normal bubbles does not build up as high as the microbubbles in the lock-in zone (Lipenkov, 2000). We used the permeation model in the Eq. (6) to model the permeation process for the normal bubbles. As for the microbubbles, we assumed steady state with the given temperatures and accumulation rates. The general characters of the firn in various depths (ages, densities, porosities, loading pressures, bubble closeoff depths) were calculated using the firn-densification heat diffusion model (Schwander et al., 1997), and they were interpolated for annual layers as for the microbubbles. We first calculated how much volume of bubbles is generated in each annual layer according to decreases in the open pore (P_{open}) with

ACPD
15, 15711–15753, 2015

depth as the following equation.

$$V_0(l+1) = (P_{\text{open}}(l) - P_{\text{open}}(l+1))(\rho_{\text{ice}} - \rho(l)) \quad (7)$$

where $V_0(l+1)$ stands for newly generated bubbles in each annual layer (Fig. 9a). The sum of all the newly generated air was set to have the air content of 6.53×10^{-5} mole mole^{-1} of ice, and then converted to the volume (m^3) with the atmospheric pressure (0.065 MPa) as in Fig. 9a. The normal bubbles start forming at ~ 40 m depth and the formation is maximum around the bubble closeoff depth of 60 to 75 m at −30 °C and 0.2 m ice yr^{-1} in the model (Fig. 9a). Then, the permeation from each annual layer was calculated according to Eq. (6). The difference from the microbubble permeation process is that the volume of the normal bubbles in each annual layer decreases according to increasing density towards deeper depth (Fig. 9a). $C(l)$ in Eq. (6) was calculated from $V_0(l)$ for each annual layer l by setting the sum of $C(l)$ as 1 (Fig. 9e). Other parameters in Eq. (6) were set to be the same as for the microbubbles.

Figure 9 shows the evolution of the normal bubble volumes, the nitrogen and argon concentrations, the $\delta Ar/N_2$ in each annual layer, and the air content and bulk $\delta Ar/N_2$ with depth at a temperature of −30 °C and an accumulation rate of 0.25 m ice yr^{-1} as for the microbubbles in Fig. 8. A new generation of the closed pore volumes in annual layers increases towards deeper depths except the last three layers, showing decreasing trapped air volume (small circles in Fig. 9a). When open pore space disappears completely, we consider the gas permeation to the open pore stops. As argon (oxygen) permeation in ice is faster than nitrogen by ~ 380 (~ 480) % at −30 °C (Fig. 7), $\delta Ar/N_2$ ($\delta O_2/N_2$) decreases when the permeation proceeds. At the temperature of −30 °C and accumulation rate of 0.25 m ice yr^{-1}, the $\delta Ar/N_2$ depletion can reach about −7 ‰ for those bubbles formed at shallow depths (Fig. 9d). However, the air contents of these bubbles are so small that the influences on the total $\delta Ar/N_2$ is limited (Fig. 9e). The depth vs. $\delta Ar/N_2$ relationship of the total air from the normal bubbles (Fig. 9e) indicates that the total $\delta Ar/N_2$ reaches the minimum of −0.56 ‰ at the beginning of the bubble closeoff depth of ~ 68 m. Then, the total $\delta Ar/N_2$ increases to −0.42 ‰ as

ACPD
15, 15711–15753, 2015

a large amount of the total air with $\delta Ar/N_2 = 0$ (after the correction for gravitation) is trapped in these depths (Fig. 9e).

6.3 Total air in bubbles

The permeation models for the normal and microbubbles were run for various firn conditions with different surface temperatures, accumulation rates, and microbubble contributions to investigate their effects on the total $\delta Ar/N_2$ (Figs. 10 and 11). Resultant air content (i.e., nitrogen, argon, and oxygen) for each annual layer from the micro- and normal bubbles were added to calculate the combined effects of the accumulation rates and temperatures on $\delta Ar/N_2$ (Fig. 10). The results show that colder (warmer) temperatures induce more (less) depletions in $\delta Ar/N_2$ for the microbubbles through thickening (thinning) of the firn, leading to higher (lower) pressures in the bubbles and longer (shorter) duration exposed to the gas loss in the firn (Figs. 10c and 11b). For the normal bubbles, the temperature changes do not appreciably influence the final $\delta Ar/N_2$ values (Figs. 10b and 11a). On the other hand, different accumulation rates induce contrasting effects on $\delta Ar/N_2$ between the normal bubbles and microbubbles. For the normal bubbles, higher (lower) accumulation rate leads to less (more) depletions in $\delta Ar/N_2$; however, for the microbubbles, higher (lower) accumulation rate induces more (less) depletions (Figs. 10c and 11b).

The sum of $\delta Ar/N_2$ in the microbubbles and normal bubbles with depth is plotted in Fig. 11c. The $\delta Ar/N_2$ minima in the firn ranges from −1 to −48 ‰ depending on the temperatures and accumulation rates. The most depleted $\delta Ar/N_2$ with a temperature of −35 °C and accumulation rate of 0.25 m ice yr^{-1} in Fig. 11c resembles the highly depleted observation-based estimates of $\delta Ar/N_2$ at 65 m (Fig. 6e). As the normal bubbles alone have only limited depletions on $\delta Ar/N_2$ with depth (Fig. 11a), the observed depleted $\delta Ar/N_2$ (Fig. 6e) is an evidence for the involvement of the microbubble permeation process. The total $\delta Ar/N_2$ at the bubble closeoff depth increases to less depleted values from the minimum (−0.6 to −1.4 ‰; Fig. 11c).

ACPD
15, 15711–15753, 2015

The calculated dependencies of the $\delta Ar/N_2$ variations on the temperature ($0.13‰\,°C^{-1}$ for an accumulation rate of $0.25\,m\,ice\,yr^{-1}$) and accumulation rate ($-0.03‰\,(0.01\,m\,ice\,yr^{-1})^{-1}$ at $-30\,°C$) with a 1 % microbubble contribution is lower than that of the observed ones ($0.72 \pm 0.1‰\,°C^{-1}$ and $-0.58 \pm 0.09‰\,(0.01\,m\,ice\,yr^{-1})^{-1}$), respectively. Considering the possibility of larger volume contributions of the microbubbles in GISP2, we calculated the microbubble permeation model with the microbubbles volume contributions of 2 and 3 % to the total air. The 3 % microbubble contribution induces more depletion in the total $\delta Ar/N_2$ (Fig. 11d). Also, the dependencies of $\delta Ar/N_2$ on temperatures and accumulation rates linearly increase to $0.38‰\,°C^{-1}$ with an accumulation rate of $0.25\,m\,ice\,yr^{-1}$, and $-0.11‰\,(0.01\,m\,ice\,yr^{-1})^{-1}$ with a temperature at $-30\,°C$, respectively. The fact that they are still lower than those of the observations may indicates even larger volume contributions from the microbubbles and/or additional amplifying processes.

We also investigated the observed lags of the $\delta Ar/N_2$ variations in GISP2 from the changes in the surface temperatures and accumulation rates by 68 and 38 years, respectively (Fig. 3). Presumably, the lags are introduced during the process of transferring surface temperature and accumulation rate signals into overloading pressure at the bubble closeoff depths. Therefore, two transient simulations were conducted using a firn densification and heat diffusion model (Goujon et al., 2003). First, the model was run with a constant temperature ($-30\,°C$) and accumulation rate ($0.2\,m\,ice\,yr^{-1}$) over thousands of years to reach an equilibrium state. Then, surface temperature and accumulation rate anomalies of $-35\,°C$ and $0.26\,m\,ice\,yr^{-1}$ for 20 years were introduced, separately (Fig. 12a). The surface anomalies of the temperature and accumulation rate were set to induce similar $\delta Ar/N_2$ changes by 3.5 ‰ from the relationship obtained by the multiple linear regressions on the $\delta Ar/N_2$ of GISP2. Then, it is found that the surface temperature anomaly takes 20 years to reach the minimum temperature at the bubble closeoff depth (Fig. 12b). The cooling induces maximum firn thickening after 56 years. The accumulation rate anomaly also induces firn thickening with an 11 years lag (Fig. 12c). Overloading pressures at the bubble closeoff depth reach similar maximum values with 85 and 21 years lags from the surface temperature and accumulation rate anomalies, respectively (Fig. 12d). Apparently, the surface temperature anomaly takes longer time to reach the maximum increase in the overloading pressure than that of the accumulation rate anomaly, which is consistent with the observation (68 and 38 years, respectively). In addition, we note that similar magnitudes of the overloading pressure anomalies were induced by the temperature and accumulation rate anomalies (Fig. 12d). Therefore, we conclude that the overloading pressure is the carrier of the surface temperature and accumulation rate signals, linking the $\delta Ar/N_2$ variations through the permeation.

7 Discussion

The processes responsible for the $\delta Ar/N_2$ variations should also play similar roles on the variations of $\delta O_2/N_2$ in ice cores but with larger magnitudes owing to the larger permeability of oxygen (Bender et al., 1995; Huber et al., 2006; Severinghaus and Battle, 2006; Battle et al., 2011). In earlier studies, causes of the $\delta O_2/N_2$ variation were attributed on the metamorphisms of surface snow induced by local insolation changes (Bender, 2002; Kawamura et al., 2007). The altered snow properties remain until the snow reaches the bubble closeoff depth and affects the preferential oxygen loss (Bender, 2002). This study demonstrated that the permeation processes in the firn can be induced by changes in the surface temperature and the accumulation rate through the changes in overloading pressure, indicating a possibility that the $\delta O_2/N_2$ variations in the orbital scale are also a result of the surface temperature and accumulation rate changes. It is noted that $\delta Ar/N_2$ in GISP2 also shows a significant positive correlation ($r = 0.37$, $p = 0.01$ after linear detrending) with the air content (Kobashi et al., 2008b) over the past 6000 years, indicating a similar link between $\delta O_2/N_2$ and air content in the orbital time scale (Raynaud et al., 2007; Lipenkov et al., 2011). As the environments of the interior of the Antarctic such as Vostok, Dome Fuji, and Dome C are radically different (very low temperatures and accumulation rates) from the Greenland Summit or NGRIP site, other mechanisms may play roles in controlling the $\delta O_2/N_2$ variations in ice cores. However, the mechanisms discussed here must be considered in future studies.

Although the gas permeation from ice is generally believed to be a mass independent process (no effects on isotopes), there are some evidences of isotopic fractionation (Bender et al., 1995; Severinghaus et al., 2003, 2009; Severinghaus and Battle, 2006; Kobashi et al., 2008b; Battle et al., 2011). Especially, poor quality ice cores often exhibit isotope fractionation (e.g, $\delta^{18}O$ and $\delta^{40}Ar$) with highly depleted $\delta O_2/N_2$ or $\delta Ar/N_2$ (Bender et al., 1995; Severinghaus et al., 2009). This mass dependent fractionation is explained by the existence of micro-cracks in poor quality ice samples that permit a relatively large air flow. On the other hand, slowly occurring gas permeations through ice crystals in good quality ice cores (e.g, NGRIP and GISP2) appear to have no effects on isotopes or are very small (Kobashi et al., 2008b; Suwa and Bender, 2008b). As small mass dependent fractionation of $\delta^{15}N$ and $\delta^{40}Ar$ during the gas permeation are similar to the gravitational fractionations (Kobashi et al., 2008b), the removal of the gravitational components also cancels the post-coring isotopic fractionations. As a result, the estimated temperature gradients in the firn are little affected by the gas loss (Kobashi et al., 2008b).

Another evidence of the isotopic fractionation during the gas loss is $\delta^{40}Ar$ enrichments in ice cores, which produces calculated temperature gradients in the firn to be lower than expected from firn modeling (Kobashi et al., 2010, 2011, 2015). The systematically higher $\delta^{40}Ar$ is believed to be caused by the processes during the bubble closeoff, but so far no clear evidence is found in the firn air studies (Huber et al., 2006; Severinghaus and Battle, 2006) except $\delta^{18}O$ of O_2 (Battle et al., 2011). If the enrichment of $\delta^{40}Ar$ occurs in the firn, it should be related with $\delta Ar/N_2$. Therefore, the corrections for the $\delta^{40}Ar$ enrichment have been applied using $\delta Ar/N_2$ (Kobashi et al., 2010, 2011; Kobashi et al., 2015) or $\delta Kr/Ar$ (Severinghaus et al., 2003), or it was corrected by a constant value (Orsi, 2013; Kobashi et al., 2015), noting that both corrections generate similar surface temperature histories (Kobashi et al., 2010, 2015). Other possible causes for the systematic offset are related to the standardizations to the atmosphere (in this case both nitrogen and argon isotopes can be affected.), or methodological differences during the extraction from ice samples (Kobashi et al., 2008b). In these cases, a constant shift should be a better solution.

For future studies on $\delta Ar/N_2$ or $\delta O_2/N_2$ in ice cores, the following suggestions should be taken into account. First, the solubility and diffusivity of argon, oxygen, and nitrogen in ice are not well constrained (Salamatin et al., 2001; Ikeda-Fukazawa et al., 2005; Bereiter et al., 2014). As precise $\delta Ar/N_2$ or $\delta O_2/N_2$ data from various ice cores are building up, the reanalyses from these cores could provide stronger constrains on the permeability. Second, although $\delta Ar/N_2$ is less susceptible to the post coring gas loss than $\delta O_2/N_2$, we have shown that the ice core preservation is critical to retrieve the original $\delta Ar/N_2$ signals. To preserve original signals, ice cores need to be stored in low temperatures (ideally $< -50\,^{\circ}C$) (Ikeda-Fukazawa et al., 2005; Bereiter et al., 2009; Landais et al., 2012), and/or to be analysed soon after the coring. Third, we also found that the use of a large amount of ice samples (600–700 g) for each analysis reduced the noises in $\delta O_2/N_2$ and $\delta Ar/N_2$ substantially (Headly, 2008), compared to the data from smaller samples in GISP2 (Suwa and Bender, 2008b). This observation emphasizes the importance of sample sizes. Fourth, observations on the bubbles in the firn and ice cores, especially on the microbubbles (e.g., numbers, volume contributions, pressure, and gas composition) are lacking, which are critical for further understanding of the permeation in the firn. Finally, the high resolution analyses (10–20 years) provided key observations for the effects of the accumulation rates and temperatures on the permeation, which warrants further similar studies along with surface temperature reconstructions.

8 Conclusion

Gas fractionations after the bubble closeoff in the firn are poorly understood processes, especially in the time domain (i.e. in ice cores). In this study, we investigated the gas

ACPD
15, 15711–15753, 2015

permeation processes in the firn and ice cores using high resolution $\delta Ar/N_2$ data from GISP2 and NGRIP ice cores for the Holocene. We found that $\delta Ar/N_2$ on the gas-age in the GISP2 ice core is significantly negatively correlated with the accumulation rate over the past 6000 years. Further, the precise surface temperatures (Kobashi et al., 2011) and accumulation rates (Alley et al., 1997; Cuffey and Clow, 1997) over the past 4000 years from the GISP2 ice core have nearly equal controls on the $\delta Ar/N_2$ variations over the past 4000 years with the sensitivities of 0.72 (‰ °C^{-1}) and −0.58 (‰ (0.01 m ice yr^{-1})$^{-1}$). To understand the processes of the $\delta Ar/N_2$ fractionation, we applied a permeation model (Ikeda-Fukazawa et al., 2005), in which air in the bubbles leak out by molecular diffusion through ice crystals, driven by the pressure gradients between the bubbles and the atmosphere.

The permeation model in the firn was applied considering two types of bubbles, "microbubbles" and "normal bubbles". Microbubbles (0.3 % of air content in the Vostok ice cores) are believed to form near the surface. Therefore, by the time when the microbubbles reach the bubble closeoff depth, they develop pressures as high as overloading ice pressure that are strongly associated with the changes in accumulation rates. On the other hand, the normal bubbles develop slightly higher pressures than that of the atmosphere at the bubble closeoff depth induced by density increases. The model indicates that $\delta Ar/N_2$ of the microbubbles is negatively correlated with the changes in accumulation rate through increases in the overloading pressures. Therefore, the observed negative correlation of $\delta Ar/N_2$ and accumulation rate can be explained by the processes on the microbubbles through the changes in the overloading pressure. Colder (warmer) temperatures are found to induce more (less) depletions in $\delta Ar/N_2$. Further understanding of the gas permeation processes in the firn may lead to a new tool to estimate the past accumulation rates or surface temperatures, and it is also important to precisely place ice core chronologies onto the orbital time scale, and to determine the timing of climate changes.

Acknowledgements. We appreciate G. Hargreaves at US National Ice Core Laboratory and J. P. Steffensen at Center for Ice and Climate, and S. Kipfstuhl at Alfred Wegener Institute for

ACPD
15, 15711–15753, 2015

ice core information. We thank S. Fujita, T. Uchida, and B. Vinther for discussion, and R. Spahni for help on firn modeling. This project is supported by KAKENHI 23710020 and 25740007 and EU Marie Curie Fellowship for T. Kobashi. This paper was written when T. Kobashi was visiting the Centre for Ice and Climate, University of Copenhagen in spring 2015, hosted by T. Blunier and B. Vinther.

References

Ahn, J. and Brook, E. J.: Atmospheric CO_2 and climate on millennial time scales during the last glacial period, Science, 322, 83–85, 2008.

Ahn, J., Headly, M., Wahlen, M., Brook, E. J., Mayewski, P. A., and Taylor, K. C.: CO_2 diffusion in polar ice: observations from naturally formed CO_2 spikes in the Siple Dome (Antarctica) ice core, J. Glaciol., 54, 685–695, 2008.

Alley, R. B., Shuman, C. A., Meese, D. A., Gow, A. J., Taylor, K. C., Cuffey, K. M., Fitzpatrick, J. J., Grootes, P. M., Zielinski, G. A., Ram, M., Spinelli, G., and Elder, B.: Visual-stratigraphic dating of the GISP2 ice core: basis, reproducibility, and application, J. Geophys. Res.-Oceans, 102, 26367–26381, 1997.

Battle, M. O., Severinghaus, J. P., Sofen, E. D., Plotkin, D., Orsi, A. J., Aydin, M., Montzka, S. A., Sowers, T., and Tans, P. P.: Controls on the movement and composition of firn air at the West Antarctic Ice Sheet Divide, Atmos. Chem. Phys., 11, 11007–11021, doi:10.5194/acp-11-11007-2011, 2011.

Bendel, V., Ueltzhöffer, K. J., Freitag, J., Kipfstuhl, S., Kuhs, W. F., Garbe, C. S., and Faria, S. H.: High-resolution variations in size, number and arrangement of air bubbles in the EPICA DML (Antarctica) ice core, J. Glaciol., 59, 972–980, 2013.

Bender, M., Sowers, T., and Lipenkov, V.: On the Concentrations of O_2, N_2, and Ar in trapped gases from ice cores, J. Geophys. Res.-Atmos., 100, 18651–18660, 1995.

Bender, M. L.: Orbital tuning chronology for the Vostok climate record supported by trapped gas composition, Earth Planet. Sc. Lett., 204, 275–289, 2002.

Bereiter, B., Schwander, J., Lüthi, D., and Stocker, T. F.: Change in CO_2 concentration and O_2/N_2 ratio in ice cores due to molecular diffusion, Geophys. Res. Lett., 36, L05703, doi:10.1029/2008GL036737, 2009.

Bereiter, B., Fischer, H., Schwander, J., and Stocker, T. F.: Diffusive equilibration of N_2, O_2 and CO_2 mixing ratios in a 1.5-million-years-old ice core, The Cryosphere, 8, 245–256, doi:10.5194/tc-8-245-2014, 2014.

Craig, H., Horibe, Y., and Sowers, T.: Gravitational separation of gases and isotopes in polar ice caps, Science, 242, 1675–1678, 1988.

Cuffey, K. M. and Clow, G. D.: Temperature, accumulation, and ice sheet elevation in central Greenland through the last deglacial transition, J. Geophys. Res.-Oceans, 102, 26383–26396, 1997.

Dahl-Jensen, D., Gundestrup, N. S., Miller, H., Watanabe, O., Johnsen, S. J., Steffensen, J. P., Clausen, H. B., Svensson, A., and Larsen, L. B.: The NorthGRIP deep drilling programme, Ann. Glaciol., 35, 1–4, 2002.

Enting, I. G.: On the use of smoothing splines to filter CO_2 data, J. Geophys. Res.-Atmos., 92, 10977–10984, 1987.

Fujita, S., Okuyama, J., Hori, A., and Hondoh, T.: Metamorphism of stratified firn at Dome Fuji, Antarctica: a mechanism for local insolation modulation of gas transport conditions during bubble close off, J. Geophys. Res.-Earth, 114, F03023, doi:10.1029/2008JF001143, 2009.

Gkinis, V., Simonsena, S. B., Buchardta, S. L., White, J. W. C., and Vinther, B. M.: Water isotope diffusion rates from the NorthGRIP ice core for the last 16,000 years – glaciological and paleoclimatic implications, Quaternary Sci. Rev., 405, 132–141, 2014.

Goujon, C., Barnola, J. M., and Ritz, C.: Modeling the densification of polar firn including heat diffusion: application to close-off characteristics and gas isotopic fractionation for Antarctica and Greenland sites, J. Geophys. Res.-Atmos., 108, 4792, doi:10.1029/2002JD003319, 2003.

Gow, A. J., Meese, D. A., Alley, R. B., Fitzpatrick, J. J., Anandakrishnan, S., Woods, G. A., and Elder, B. C.: Physical and structural properties of the Greenland Ice Sheet Project 2 ice core: a review, J. Geophys. Res.-Oceans, 102, 26559–26575, 1997.

Headly, M. A.: Krypton and xenon in air trapped in polar ice cores: paleo-atmospheric measurements for estimating past mean ocean temperature and summer snowmelt frequency, PhD, University of California, San Diego, La Jolla, 247 pp., 2008.

Herron, M. M. and Langway, C. C.: Firn densification: an empirical model, J. Glaciol., 25, 373–385, 1980.

Huber, C., Beyerle, U., Leuenberger, M., Schwander, J., Kipfer, R., Spahni, R., Severinghaus, J. P., and Weiler, K.: Evidence for molecular size dependent gas fractionation in firn air

ACPD
15, 15711–15753, 2015

derived from noble gases, oxygen, and nitrogen measurements, Earth Planet. Sc. Lett., 243, 61–73, 2006.
Ikeda-Fukazawa, T. and Kawamura, K.: Effects of ions on dynamics of ice surface, Chem. Phys. Lett., 417, 561–565, 2006.
Ikeda-Fukazawa, T., Hondoh, T., Fukumura, T., Fukazawa, H., and Mae, S.: Variation in N_2/O_2 ratio of occluded air in Dome Fuji antarctic ice, J. Geophys. Res.-Atmos., 106, 17799–17810, 2001.
Ikeda-Fukazawa, T., Kawamura, K., and Hondoh, T.: Mechanism of molecular diffusion in ice crystals, Mol. Simulat., 30, 973–979, 2004.
Ikeda-Fukazawa, T., Fukumizu, K., Kawamura, K., Aoki, S., Nakazawa, T., and Hondoh, T.: Effects of molecular diffusion on trapped gas composition in polar ice cores, Earth Planet. Sc. Lett., 229, 183–192, 2005.
Ikeda, T., Fukazawa, H., Mae, S., Pepin, L., Duval, P., Champagnon, B., Lipenkov, V. Y., and Hondoh, T.: Extreme fractionation of gases caused by formation of clathrate hydrates in Vostok Antarctic ice, Geophys. Res. Lett., 26, 91–94, 1999.
Ito, H. and Minobe, S.: Data Analysis for Meteorology and Physical Oceanography, Meteorological Research Note, 233, Meteorological Society of Japan, 263 pp., Tokyo, 2010.
Kawamura, K., Severinghaus, J. P., Ishidoya, S., Sugawara, S., Hashida, G., Motoyama, H., Fujii, Y., Aoki, S., and Nakazawa, T.: Convective mixing of air in firn at four polar sites, Earth Planet. Sc. Lett., 244, 672–682, 2006.
Kawamura, K., Parrenin, F., Lisiecki, L., Uemura, R., Vimeux, F., Severinghaus, J. P., Hutterli, M. A., Nakazawa, T., Aoki, S., and Jouzel, J.: Northern Hemisphere forcing of climatic cycles in Antarctica over the past 360 000 years, Nature, 448, 912–916, 2007.
Kobashi, T., Severinghaus, J., Brook, E. J., Barnola, J. M., and Grachev, A.: Precise timing and characterization of abrupt climate change 8200 years ago from air trapped in polar ice, Quarternary Sci. Rev., 26, 1212–1222, doi:10.1016/j.quascirev.2007.01.009, 2007.
Kobashi, T., Severinghaus, J. P., and Barnola, J. M.: $4\pm1.5\,^{\circ}$C abrupt warming 11,270 years ago identified from trapped air in Greenland ice, Earth Planet. Sc. Lett., 268, 397–407, 2008a.
Kobashi, T., Severinghaus, J. P., and Kawamura, K.: Argon and nitrogen isotopes of trapped air in the GISP2 ice core during the Holocene epoch (0–11,600 B. P.): methodology and implications for gas loss processes, Geochim. Cosmochim. Ac., 72, 4675–4686, 2008b.

Kobashi, T., Severinghaus, J. P., Barnola, J. M., Kawamura, K., Carter, T., and Nakaegawa, T.: Persistent multi-decadal Greenland temperature fluctuation through the last millennium, Climatic Change, 100, 733–756, 2010.

Kobashi, T., Kawamura, K., Severinghaus, J. P., Barnola, J.-M., Nakaegawa, T., Vinther, B. M., Johnsen, S. J., and Box, J. E.: High variability of Greenland surface temperature over the past 4000 years estimated from trapped air in an ice core, Geophys. Res. Lett., 38, doi:10.1029/2011GL049444, 2011.

Kobashi, T., Shindell, D. T., Kodera, K., Box, J. E., Nakaegawa, T., and Kawamura, K.: On the origin of multidecadal to centennial Greenland temperature anomalies over the past 800 yr, Clim. Past, 9, 583–596, doi:10.5194/cp-9-583-2013, 2013.

Kobashi, T., Box, J. E., Vinther, B. M., Goto-Azuma, K., Blunier, T., White, J. W. C., Nakaegawa, T., and Andresen, C. S.: Modern solar maximum forced late 20th century Greenland cooling, Geophys. Res. Lett., submitted, 2015.

Landais, A., Dreyfus, G., Capron, E., Pol, K., Loutre, M. F., Raynaud, D., Lipenkov, V. Y., Arnaud, L., Masson-Delmotte, V., Paillard, D., Jouzel, J., and Leuenberger, M.: Towards orbital dating of the EPICA Dome C ice core using $\delta O_2/N_2$, Clim. Past, 8, 191–203, doi:10.5194/cp-8-191-2012, 2012.

Lipenkov, V. Y.: Air bubbles and air-hydrate crystals in the Vostok ice core, in: Physics of Ice Core Records, 327–358, Hokkaido University Press, Sapporo, 2000.

Lipenkov, V. Y., Raynaud, D., Loutre, M., and Duval, P.: On the potential of coupling air content and O_2/N_2 from trapped air for establishing an ice core chronology tuned on local insolation, Quaternary Sci. Rev., 30, 3280–3289, 2011.

Lomonaco, R., Albert, M., and Baker, I.: Microstructural evolution of fine-grained layers through the firn column at Summit, Greenland, J. Glaciol., 57, 755–762, 2011.

Matzl, M. and Schneebeli, M.: Measuring specific surface area of snow by near-infrared photography, J. Glaciol., 52, 558–564, 2006.

Mitchell, L. E., Buizert, C., Brook, E. J., Breton, D. J., Fegyveresi, J., Baggenstos, D., Orsi, A., Severinghaus, J., Alley, R. B., Albert, M., Rhodes, R. H., McConnell, J. R., Sigl, M., Maselli, O., Gregory, S., and Ahn, J.: Observing and modeling the influence of layering on bubble trapping in polar firn, J. Geophys. Res.-Atmos., 120, 2558–2574, doi:10.1002/2014JD022766, 2015.

Orsi, A. J.: Temperature reconstruction at the West Antarctic Ice Sheet Divide, for the last millennium from the combination of borehole temperature and inert gas isotope measurements, PhD Thesis, University of California, San Diego, La Jolla, CA, 243 pp., 2013.

Petit, J. R., Jouzel, J., Raynaud, D., Barkov, N., Barnola, J., Basile, I., Bender, M., Chappellaz, J., Davis, M., and Delaygue, G.: Climate and atmospheric history of the past 420,000 years from the Vostok ice core, Antarctica, Nature, 399, 429–436, 1999.

Raynaud, D., Lipenkov, V., Lemieux-Dudon, B., Duval, P., Loutre, M. F., and Lhomme, N.: The local insolation signature of air content in Antarctic ice. A new step toward an absolute dating of ice records, Earth Planet. Sc. Lett., 261, 337–349, 2007.

Salamatin, A. N., Lipenkov, V. Y., Ikeda-Fukazawa, T., and Hondoh, T.: Kinetics of air–hydrate nucleation in polar ice sheets, J. Cryst. Growth, 223, 285–305, 2001.

Schwander, J.: The transformation of snow to ice and the occlusion of gases, in: Glaciers and Ice Sheets, edited by: Oeschger, H., and Langway Jr., C. C., John Wiley, New York, 53–67, 1989.

Schwander, J.: Firn Air Sampling, Field Report, North GRIP 2001, Bern, 2001.

Schwander, J., Barnola, J. M., Andrie, C., Leuenberger, M., Ludin, A., Raynaud, D., and Stauffer, B.: The age of the air in the firn and the ice at Summit, Greenland, J. Geophys. Res.-Atmos., 98, 2831–2838, 1993.

Schwander, J., Sowers, T., Barnola, J. M., Blunier, T., Fuchs, A., and Malaize, B.: Age scale of the air in the summit ice: implication for glacial–interglacial temperature change, J. Geophys. Res.-Atmos., 102, 19483–19493, 1997.

Seierstad, I. K., Abbott, P. M., Bigler, M., Blunier, T., Bourne, A. J., Brook, E., Buchardt, S. L., Buizert, C., Clausen, H. B., Cook, E., Dahl-Jensen, D., Davies, S. M., Guillevic, M., Johnsen, S. J., Pedersen, D. S., Popp, T. J., Rasmussen, S. O., Severinghaus, J., Svensson, A., and Vinther, B. M.: Consistently dated records from the Greenland GRIP, GISP2 and NGRIP ice cores for the past 104 ka reveal regional millennial-scale δ18O gradients with possible Heinrich event imprint, Quaternary Sci. Rev., 106, 29–16, doi:10.1016/j.quascirev.2014.10.032, 2014.

Severinghaus, J. P. and Battle, M. O.: Fractionation of gases in polar lee during bubble close-off: new constraints from firn air Ne, Kr and Xe observations, Earth Planet. Sc. Lett., 244, 474–500, 2006.

Severinghaus, J. P., Sowers, T., Brook, E. J., Alley, R. B., and Bender, M. L.: Timing of abrupt climate change at the end of the Younger Dryas interval from thermally fractionated gases in polar ice, Nature, 391, 141–146, 1998.

Severinghaus, J. P., Grachev, A., Luz, B., and Caillon, N.: A method for precise measurement of argon 40/36 and krypton/argon ratios in trapped air in polar ice with applications to past firn thickness and abrupt climate change in Greenland and at Siple Dome, Antarctica, Geochim. Cosmochim. Ac., 67, 325–343, 2003.

Severinghaus, J. P., Beaudette, R., Headly, M., Taylor, K., and Brook, E.: Oxygen-18 of O_2 records the impact of abrupt climate change on the terrestrial biosphere, Science, 324, 1431–1434, 2009.

Spahni, R., Chappellaz, J., Stocker, T. F., Loulergue, L., Hausammann, G., Kawamura, K., Fluckiger, J., Schwander, J., Raynaud, D., Masson-Delmotte, V., and Jouzel, J.: Atmospheric methane and nitrous oxide of the late Pleistocene from Antarctic ice cores, Science, 310, 1317–1321, 2005.

Stuiver, M., Grootes, P. M., and Braziunas, T. F.: The GISP2 δ^{18}O climate record of the past 16 500 years and the role of the sun, ocean, and volcanoes, Quaternary Res., 44, 341–354, 1995.

Suwa, M. and Bender, M. L.: Chronology of the Vostok ice core constrained by O_2/N_2 ratios of occluded air, and its implication for the Vostok climate records, Quaternary Sci. Rev., 27, 1093–1106, 2008a.

Suwa, M. and Bender, M. L.: O2/N2 ratios of occluded air in the GISP2 ice core, J. Geophys. Res.-Atmos., 113, D11119, doi:10.1029/2007JD009589, 2008b.

Ueltzhöffer, K. J., Bendel, V., Freitag, J., Kipfstuhl, S., Wagenbach, D., Faria, S. H., and Garbe, C. S.: Distribution of air bubbles in the EDML and EDC (Antarctica) ice cores, using a new method of automatic image analysis, J. Glaciol., 56, 339–348, 2010.

Vinther, B. M., Clausen, H. B., Johnsen, S. J., Rasmussen, S. O., Andersen, K. K., Buchardt, S. L., Dahl-Jensen, D., Seierstad, I. K., Siggaard-Andersen, M. L., and Steffensen, J. P.: A synchronized dating of three Greenland ice cores throughout the Holocene, J. Geophys. Res.-Atmos., 111, D13102, doi:10.1029/2005JD006921, 2006.

Vinther, B. M., Buchardt, S. L., Clausen, H. B., Dahl-Jensen, D., Johnsen, S. J., Fisher, D. A., Koerner, R. M., Raynaud, D., Lipenkov, V., Andersen, K. K., Blunier, T., Rasmussen, S. O., Steffensen, J. P., and Svensson, A. M.: Holocene thinning of the Greenland ice sheet, Nature, 461, 385–388, 2009.

ACPD
15, 15711–15753, 2015

Post bubble-closeoff fractionation of gases in polar firn and ice cores

T. Kobashi et al.

Von Storch, H., Zorita, E., Jones, J. M., Dimitriev, Y., González-Rouco, F., and Tett, S. F.: Reconstructing past climate from noisy data, Science, 306, 679–682, 2004.
White, J. W. C., Barlow, L. K., Fisher, D., Grootes, P., Jouzel, J., Johnsen, S. J., Stuiver, M., and Clausen, H.: The climate signal in the stable isotopes of snow from Summit, Greenland: results of comparisons with modern climate observations, J. Geophys. Res.-Oceans, 102, 26425–26439, 1997.

ACPD
15, 15711–15753, 2015

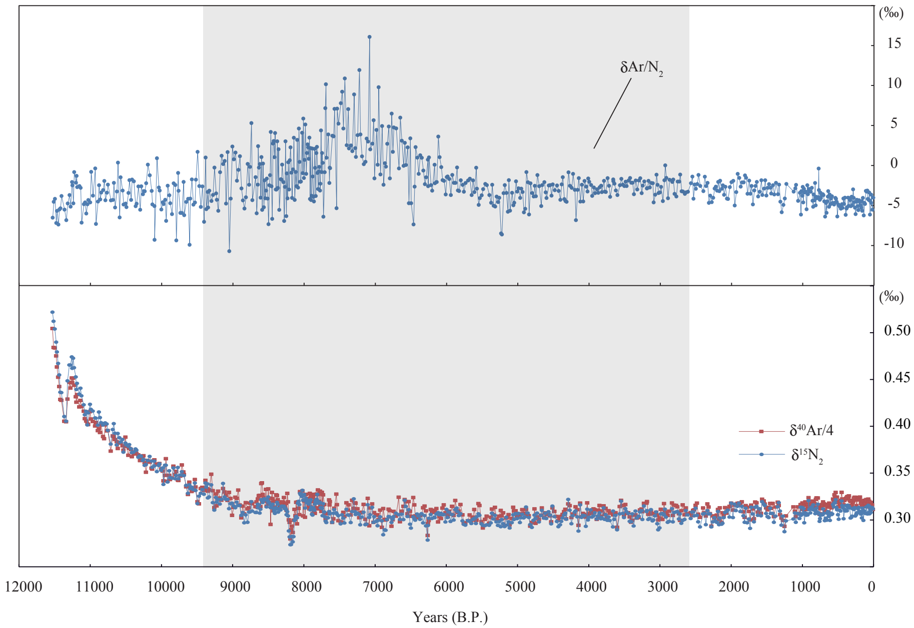

Figure 1. δ^{15}N, δ^{40}Ar/4, and δAr/N_2 from the GISP2 ice core over the Holocene (Kobashi et al., 2008b). The grey area indicates the brittle zone (Gow et al., 1997).

ACPD
15, 15711–15753, 2015

Post bubble-closeoff fractionation of gases in polar firn and ice cores

T. Kobashi et al.

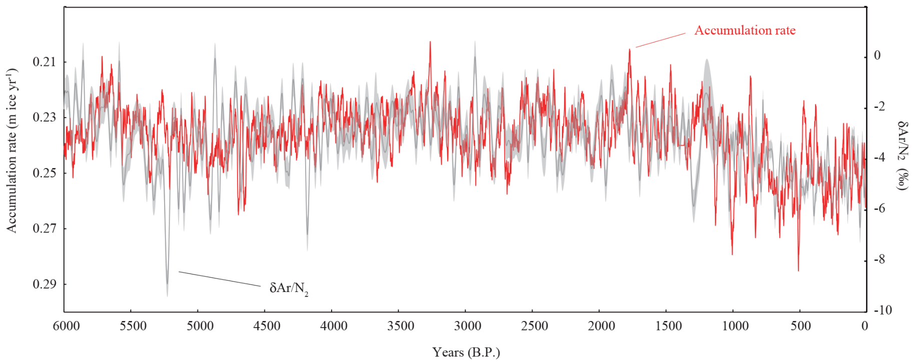

Figure 2. $\delta Ar/N_2$ and accumulation rate in GISP2 over the past 6000 years. A spline with a 31 years cut off period (grey line) was applied to the $\delta Ar/N_2$ data, and a 1σ error bound (shown) was estimated by 1000 times of Monte Carlo simulation. Accumulation rate (m ice yr^{-1}) (red line) was filtered by 31 years RMs. Note that the *y* axis for the accumulation rate is reversed.

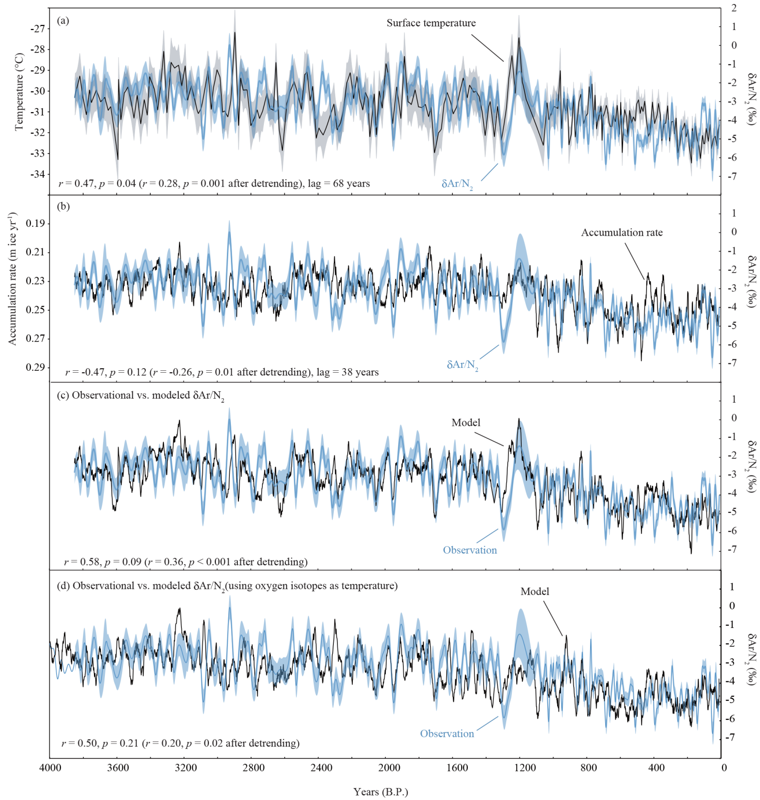

Figure 3. The observed and modeled δAr/N$_2$ from the GISP2 ice core over the past 4000 years, compared with the surface temperature and accumulation rate. **(a)** δAr/N$_2$ and surface temperatures (Kobashi et al., 2011). **(b)** δAr/N$_2$ and accumulation rates in 21 years RMs (Alley et al., 1997; Cuffey and Clow, 1997). **(c)** Observed and modeled δAr/N$_2$ from the multiple linear regression (see text). **(d)** Observed and modeled δAr/N$_2$ of the multiple linear regression using $\delta^{18}O_{ice}$ as a temperature proxy (see text). Error bounds are 1σ.

ACPD
15, 15711–15753, 2015

Post bubble-closeoff fractionation of gases in polar firn and ice cores

T. Kobashi et al.

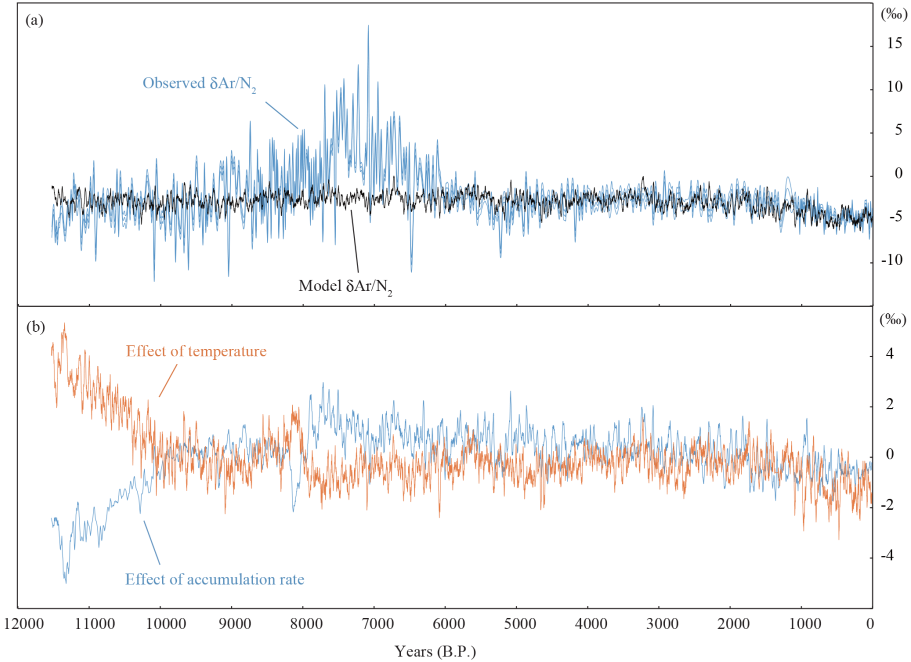

Figure 4. The observed and modeled $\delta Ar/N_2$ over the Holocene **(a)**, and decomposition of $\delta Ar/N_2$ into the effects of the accumulation rates and temperatures **(b)**.

ACPD
15, 15711–15753, 2015

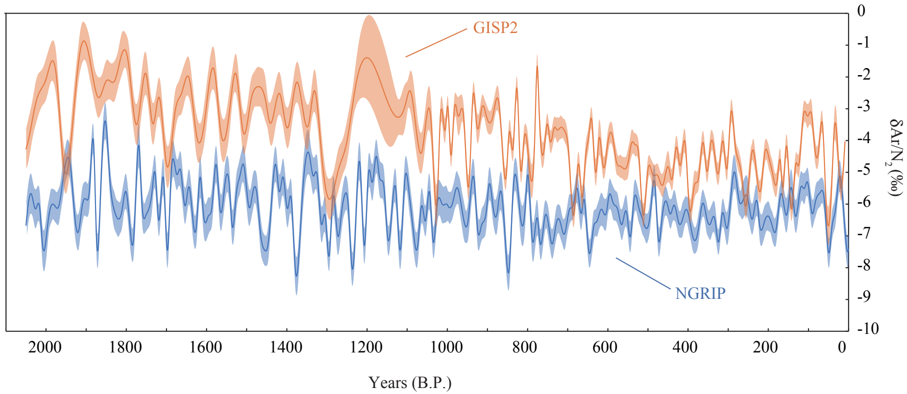

Figure 5. The observed $\delta Ar/N_2$ for GISP2 and NGRIP over the past 2100 years. Spline fits (Enting, 1987) were applied with a 20 years cut off period, and 1σ uncertainties bounds (shown) were estimated by 1000 Monte Carlo simulations.

ACPD
15, 15711–15753, 2015

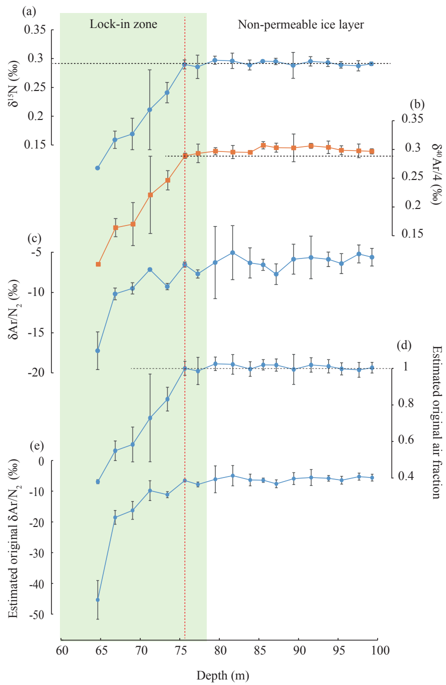

Figure 6. $\delta^{15}N$, $\delta^{40}Ar/4$, and $\delta Ar/N_2$ in the NGRIP ice core from shallower depths (60–100 m). **(a)** $\delta^{15}N$, **(b)** $\delta^{40}Ar/4$, **(c)** $\delta Ar/N_2$, **(d)** estimated original air fractions, **(e)** estimated original $\delta Ar/N_2$. The estimated original air fractions relative to the value at 75.6 m was calculated with a mass balance calculation, assuming that $\delta^{15}N$ in the lock-in zone is constant with the value of 0.289 ‰ at 75.6 m and $\delta^{15}N$ of the ambient air is 0.0 ‰. From the calculated original air fraction, the original $\delta Ar/N_2$ were estimated again by the mass balance calculation, assuming the ambient $\delta Ar/N_2$ is 0.0 ‰. Green shaded area indicates the lock-in zone. Dotted lines in $\delta^{15}N$, $\delta^{40}Ar$, and estimated original air fraction are the values at 75.6 m. Error bounds are 2σ.

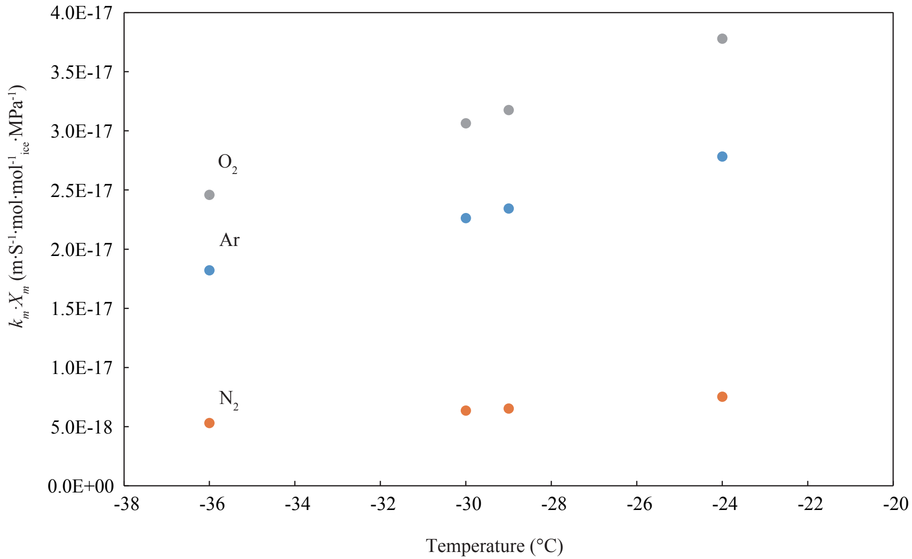

Figure 7. $k_m \cdot X_m$ for oxygen, argon, and nitrogen at different temperatures.

ACPD
15, 15711–15753, 2015

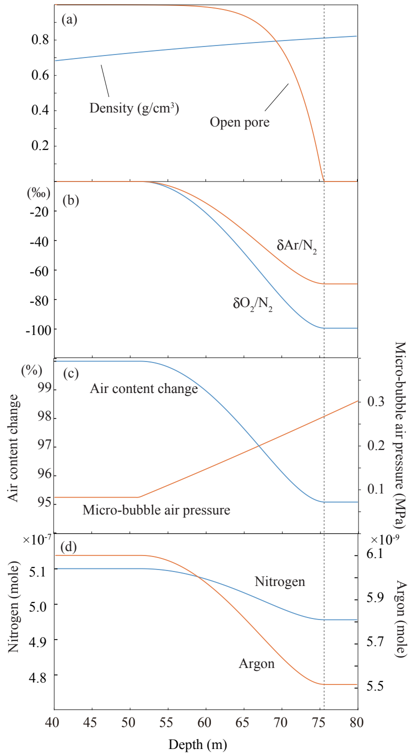

Figure 8. Simulated $\delta Ar/N_2$ vs. depth relationship in the microbubbles with a temperature of $-30\,^{\circ}C$, accumulation rate of 0.25 m ice yr^{-1}, and microbubble contribution 1 %. **(a)** Density and open pore. **(b)** $\delta Ar/N_2$ and $\delta O_2/N_2$. **(c)** Air content change and air pressure in the microbubbles. **(d)** Nitrogen and argon concentrations.

ACPD
15, 15711–15753, 2015

Post bubble-closeoff fractionation of gases in polar firn and ice cores

T. Kobashi et al.

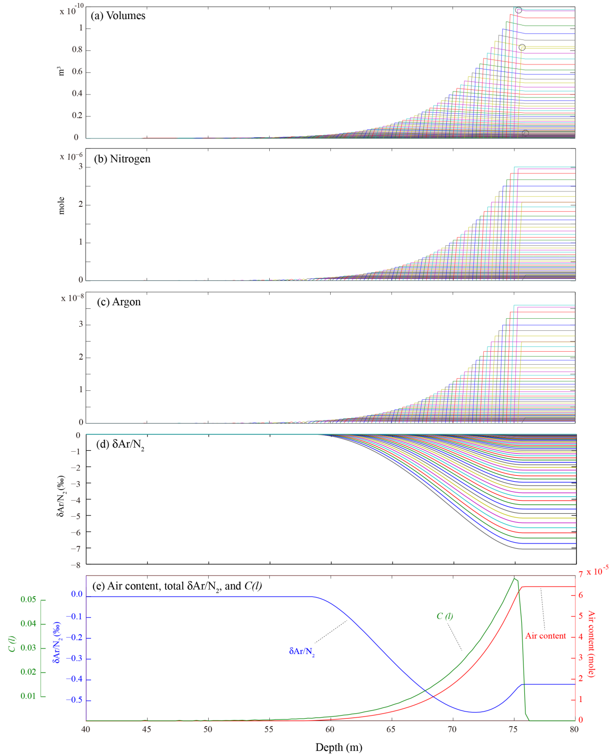

Figure 9. The simulated $\delta Ar/N_2$ changes in annual layers with depth for the normal bubbles with temperature of −30 °C and accumulation rate of 0.25 m ice yr^{-1}, and parameters (volumes and $C(l)$) for the calculation. **(a)** Changes in volumes of the normal bubbles in annual layers. Three circles show decreasing trapped air volumes with depth (see text). **(b)** Nitrogen concentrations as in **(a)**. **(c)** Argon concentrations as in **(a)**. **(d)** $\delta Ar/N_2$ as in **(a)**. **(e)** Air content, $\delta Ar/N_2$, and $C(l)$ for the bulk normal bubbles.

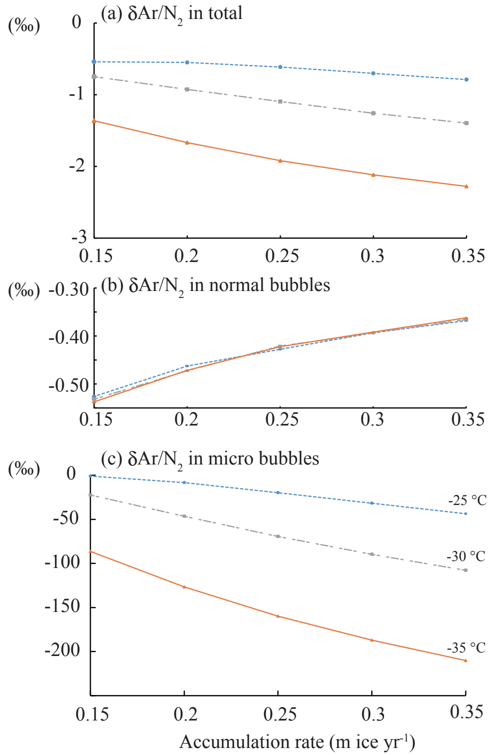

Figure 10. The simulated δAr/N$_2$ fractionation in response to different temperatures and accumulation rates for the total, normal bubbles, and micro-bubbles after all the fractionations in the firn. Microbubble contribution was set to 1 %. **(a)** Total δAr/N$_2$. **(b)** δAr/N$_2$ in the normal bubbles. **(c)** δAr/N$_2$ in the microbubbles. Circles, rectangles, and triangles indicate values at −25, −30, and −35 °C, respectively.

ACPD
15, 15711–15753, 2015

Post bubble-closeoff fractionation of gases in polar firn and ice cores

T. Kobashi et al.

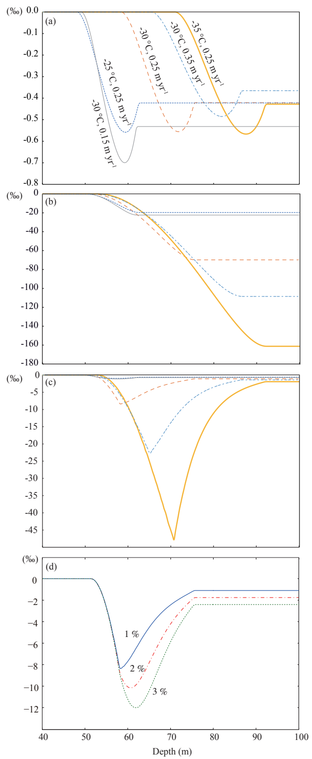

Figure 11. The simulated δAr/N_2 fractionation with depth in the firn for the normal and microbubbles with different temperatures and accumulation rates. Microbubble contribution was set to 1 % except the panel **(d)**. **(a)** δAr/N_2 changes in the normal bubbles. **(b)** δAr/N_2 changes in the microbubbles. **(c)** δAr/N_2 changes in all the bubbles. Setting for the temperatures and accumulation rates were defined in the panel **(a)**. **(d)** Influences of variable microbubble volumes (1 to 3 %) to the total δAr/N_2 with a temperature of −30 °C and accumulation rate of 0.25 m ice yr^{-1}.

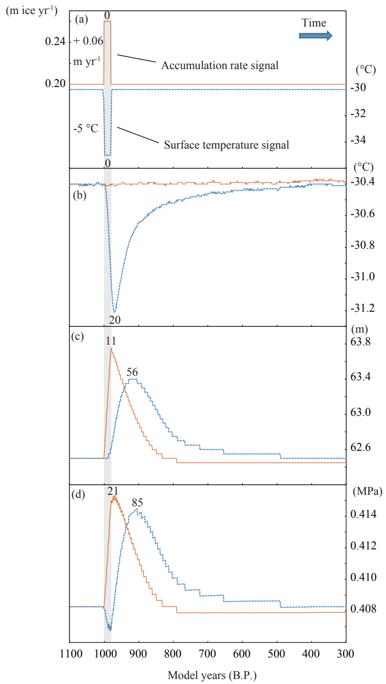

Figure 12. Two model experiments for the effects of surface temperatures and accumulation rates on the overloading pressure at the bubble closeoff depth. **(a)** Accumulation rates (20 m ice yr^{-1}) and surface temperatures (−30 °C) with 20 years anomalies for the model year 1000–981 BP When one input was used for an experiment, the other was set constant. Zero in the panel **(a)** indicates the central year (model year 990 BP) of the anomalies. **(b)** Temperature changes at the bubble closeoff depth. **(c)** Changes in the firn thickness. **(d)** Overloading pressures at the bubble closeoff depth. The orange line is the accumulation rate experiment, and the blue line is the temperature experiment. Numbers on peaks in **(b–d)** are lags in years from the central year of the initial anomalies in the panel **(a)**.